

Volume preserving image registration via a post-processing stage

Reinhard Hameeteman¹, Jifke F. Veenland¹, and Wiro J. Niessen^{1,2}

¹ Biomedical Imaging Group Rotterdam, Erasmus MC - University Medical Center Rotterdam Departments of Radiology and Medical Informatics, Dr. Molewaterplein 50, 3015 GE Rotterdam, The Netherlands

² Quantitative Imaging Group, Department of Imaging Science and Technology, Faculty of Applied Sciences, Delft University of Technology, Lorentzweg 1, 2628 CJ Delft, The Netherlands

ABSTRACT

In this paper a method to remove the divergence from a vector field is presented. When applied to a displacement field, this will remove all local compression and expansion. The method can be used as a post-processing step for (unconstrained) registered images, when volume changes in the deformation field are undesired. The method involves solving Poisson's equation for a large system. Algorithms to solve such systems include Fourier analysis and Cyclic Reduction. These solvers are vastly applied in the field of fluid dynamics, to compensate for numerical errors in calculated velocity fields. The application to medical image registration as described in this paper, has to our knowledge not been done before. To show the effect of the method, it is applied to the registration of both synthetic data and dynamic MR series of the liver. The results show that the divergence in the displacement field can be reduced by a factor of 10 – 1000 and that the accuracy of the registration increases.

Keywords: Registration

1. INTRODUCTION

Image registration is a key technology in the analysis of (bio)medical imaging data in clinical practice and biomedical research. By establishing spatial correspondence between images it enables, a.o., multi-modality visualization, tracking of changes over time, and comparison between patient groups. A very common approach to image registration is the optimisation of a similarity metric with respect to the parameters that describe the transformation between two images. One of the most important aspects of a registration algorithm is the choice of the right constraints on the deformation field. For instance, no folding should be allowed and solid structures should only be transformed in a rigid manner.

For most applications, many structures in the human body can be considered incompressible, which leads to the demand of a registration that does not allow for volume changes within those structures. If the registration of such structures would be perfect, *i.e.* when the same structures are exactly mapped onto each other, there would be no volume changes present in the resulting displacement field. However most times there is a need to apply some constraints in order to avoid undesired volume changes. Several specialised volume preserving registration methods have been developed.^{1,2} For a more general discussion on volume preserving regularisation terms, see.³ Sometimes it is hard to incorporate such constraints within the registration framework. Moreover, using an incompressibility constraint during the registration may lead to a considerable slow down of the registration when derivative information of the similarity metric can no longer be analytically calculated. To avoid these issues we propose a post-processing step to remove any volume changes that are present in the displacement field obtained with the registration algorithm.

2. METHOD

In this section we introduce the proposed method to remove volume changes in a displacement field. We start by giving a general description of the followed procedure. This leads to the description of the Poisson equation that needs to be solved. In the subsequent subsections two techniques that can be used to solve this equation are introduced, after which the section is concluded with some remarks on other solvers.

2.1 Correcting a vector field for volume changes

In mathematical terms an incompressibility constraint is equal to the demand for zero divergence in every point of the displacement field:

$$\nabla \cdot \vec{u}(x, y, z) = 0 \quad (1)$$

A displacement field obeying this rule is called solenoidal. To make a displacement field solenoidal, we try to find a correction field, $\vec{\varepsilon}(x, y, z)$, that makes the original field, $\vec{u}(x, y, z)$ solenoidal:

$$\nabla \cdot [\vec{u}(x, y, z) - \vec{\varepsilon}(x, y, z)] = 0 \quad (2)$$

By searching for a field that can be described as the gradient of some potential field the coupled partial vector equations are converted into a single differential:

$$\vec{\varepsilon}(x, y, z) = \nabla\phi(x, y, z) \quad (3)$$

Equation (2) and (3) together lead to

$$\Delta\phi(x, y, z) = \nabla \cdot \vec{u}(x, y, z) \quad (4)$$

Note that Equation (4) can also be obtained by using the Helmholtz decomposition theorem, which states that any smooth vector field can be decomposed into a solenoidal (divergence free) field and an irrotational (curl free) field:

$$F = -\nabla\xi + \nabla \times A \quad (5)$$

where $\nabla \cdot A = \nabla \cdot (\vec{u} - \vec{\varepsilon}) = 0$ and $\nabla \times \xi = 0$

Equation (4) is a Poisson equation, since $\nabla \cdot \vec{u}(x, y, z) = g(x, y, z)$ is a scalar potential that can be calculated from $\vec{u}(x, y, z)$. In order to obtain a zero centred field we can subtract the mean value from $\vec{\varepsilon}(x, y, z)$, because adding a constant vector to a vector field, does not change its divergence: thus any field $\vec{\varepsilon}(x, y, z) + \vec{c}$ also satisfies Equation (2).

Using discrete notation with sampling interval δ and central finite difference approximation of the second derivative operator, Equation (4) turns into:

$$\begin{aligned} &\phi_{p-1,q,r} - 2\phi_{p,q,r} + \phi_{p+1,q,r} + \\ &\phi_{p,q-1,r} - 2\phi_{p,q,r} + \phi_{p,q+1,r} + \\ &\phi_{p,q,r-1} - 2\phi_{p,q,r} + \phi_{p,q,r+1} = \delta^2 g_{p,q,r} \end{aligned} \quad (6)$$

where for ease of notation we have taken the sampling interval δ to be equal in all directions and $g(x, y, z)$ is sampled using the same intervals, so $\phi_{p,q,r} = \phi(p\delta, q\delta, r\delta)$ and $g_{p,q,r} = g(p\delta, q\delta, r\delta)$.

Equation (6) represents a very large system of equations. In fact it results in a equation for every point in the original field. So when the original field is defined at 256*256*64 locations, this will result in a system of 4.2 million equations.

Solving Poisson's equation for such large systems is a commonly faced problem in the field of fluid dynamics. Numerically calculated velocity fields often have some imperfections in them: although fluids are incompressible the calculated velocity fields are not solenoidal. To remove the divergence from the velocity field the same method as described in this section, is used. Solving the resulting Poisson equation is done by using two techniques: Fourier Analysis and Cyclic Reduction^{4,5}. These techniques are described in the following sections.

2.2 Fourier Analysis

We will start by looking at a 1D case to understand the procedure and then present the formulas for the full 3D case, which is a straightforward extension. In one dimension the Poisson Equation (6) is reduced to:

$$\frac{\phi_{p-1} - 2\phi_p + \phi_{p+1}}{\delta^2} = g_p \quad (7)$$

Using the inverse Fourier transform ϕ_p and g_p can be expanded as:

$$\phi_p = \frac{1}{L} \sum_{l=1}^L \hat{\phi}_l e^{-2\pi i p l / L}, g_p = \frac{1}{L} \sum_{l=1}^L \hat{g}_l e^{-2\pi i p l / L} \quad (8)$$

where $\hat{\phi}_l$ and \hat{g}_l denote the Discrete Fourier Transform (DFT) coefficients. Combining equations (7) and (8) and rearranging terms results in:

$$\begin{aligned} & \frac{1}{L} \sum_{l=1}^L \hat{\phi}_l e^{-2\pi i p l / L} \left(\frac{e^{2\pi i l / L} - 2 + e^{-2\pi i l / L}}{\delta^2} \right) \\ &= \frac{1}{L} \sum_{l=1}^L \hat{g}_l e^{-2\pi i p l / L} \end{aligned} \quad (9)$$

which gives us a relation between the unknown $\hat{\phi}_l$ and the \hat{g}_l :

$$2\hat{\phi}_l \frac{\cos(2\pi l / L) - 1}{\delta^2} = \hat{g}_l \quad (10)$$

Because the \hat{g}_l can be calculated from g_p by means of the DFT and the ϕ_p can be calculated from $\hat{\phi}_l$ using the inverse DFT from Equation (8), the 1D problem of Equation (7) is solved.

The extension to the 3D case is straightforward. In isotropically sampled images this leads to the following expression for the Fourier coefficients $\hat{\phi}_{l,m,n}$

$$\begin{aligned} 2\hat{\phi}_{l,m,n} \left(\cos\left(\frac{2\pi l}{L}\right) + \cos\left(\frac{2\pi m}{M}\right) \right. \\ \left. + \cos\left(\frac{2\pi n}{N}\right) - 3 \right) = \delta^2 \hat{g}_{l,m,n} \end{aligned} \quad (11)$$

Using the 3D (inverse) Fourier transforms the unknowns $\phi_{p,q,r}$ can now be computed.

Solving the Poisson equation using Fourier analysis thus involves three steps:

1. Compute the Fourier transform of g_p . This can be done using the Fast Fourier Transform.
2. Use Equation (11) to compute the frequency components $\hat{\phi}_{l,m,n}$.
3. Compute $\phi_{p,q,r}$ using the inverse DFT.

2.3 Cyclic reduction

Cyclic reduction is best understood in 1D, but the generalisation to higher dimensions only becomes straightforward after the extension to 2D. To reduce notational complexity we make two additional simplifications with respect to the sampling distance δ and the number of elements P in each dimension: $\delta = 1$ and $P = 2^k, k \in \mathbb{R}$. Writing Equation (7) using matrix notation then gives:

$$\begin{pmatrix} -2 & 1 & & & & \\ 1 & -2 & 1 & & & \\ & & \ddots & \ddots & \ddots & \\ & & & 1 & -2 & 1 \\ & & & & 1 & -2 \end{pmatrix} \begin{pmatrix} \phi_1 \\ \phi_2 \\ \vdots \\ \phi_{P-1} \\ \phi_P \end{pmatrix} = \begin{pmatrix} g_1 \\ g_2 \\ \vdots \\ g_{P-1} \\ g_P \end{pmatrix} \quad (12)$$

or,

$$\mathbf{K}_{1D} \vec{\Phi} = \vec{G} \quad (13)$$

When we multiply row i of the matrix in Equation (12) by 2 and add the surrounding rows we see that the elements of the columns $i - 1$ and $i + 1$ are eliminated. By performing this operation for all even rows, all elements in the odd columns are eliminated and the result is a half-sized system. This procedure is known as odd-even reduction.

Generalising to 2D the ordering of the elements must be specified. We use the default row major ordering where a grid is put in the vector row by row. The matrix of Equation (13) now takes the form of a block tridiagonal matrix \mathbf{K}_{2D} :

$$\begin{pmatrix} \mathbf{A} & \mathbf{I} & & & & \\ \mathbf{I} & \mathbf{A} & \mathbf{I} & & & \\ & & \ddots & \ddots & \ddots & \\ & & & \mathbf{I} & \mathbf{A} & \mathbf{I} \\ & & & & \mathbf{I} & \mathbf{A} \end{pmatrix} \begin{pmatrix} \phi_1 \\ \phi_2 \\ \vdots \\ \phi_Q \end{pmatrix} = \begin{pmatrix} \mathbf{g}_1 \\ \mathbf{g}_2 \\ \vdots \\ \mathbf{g}_Q \end{pmatrix} \quad (14)$$

where $\mathbf{A} = \mathbf{K}_{1D} - 2\mathbf{I}$ and ϕ_i and \mathbf{g}_i are \mathbf{L} sized vectors containing the i^{th} rows of ϕ and g respectively. On this system we can again apply odd-even reduction by multiplying the odd rows by \mathbf{I} , the even rows by $-\mathbf{A}$ and adding three consecutive rows, ending up with:

$$\begin{pmatrix} 2\mathbf{I}^2 - \mathbf{A}^2 & \mathbf{I}^2 & & & & \\ \mathbf{I}^2 & 2\mathbf{I}^2 - \mathbf{A}^2 & \mathbf{I}^2 & & & \\ & & \ddots & \ddots & \ddots & \\ & & & \mathbf{I}^2 & 2\mathbf{I}^2 - \mathbf{A}^2 & \mathbf{I}^2 \\ & & & & \mathbf{I}^2 & 2\mathbf{I}^2 - \mathbf{A}^2 \end{pmatrix} \times \begin{pmatrix} \phi_2 \\ \phi_4 \\ \vdots \\ \vdots \\ \phi_{Q-2} \end{pmatrix} = \begin{pmatrix} \mathbf{I}\mathbf{g}_1 - \mathbf{A}\mathbf{g}_2 + \mathbf{I}\mathbf{g}_3 & \mathbf{I}\mathbf{g}_3 - \mathbf{A}\mathbf{g}_4 + \mathbf{I}\mathbf{g}_5 \\ \vdots \\ \vdots \\ \mathbf{I}\mathbf{g}_{Q-3} - \mathbf{A}\mathbf{g}_{Q-2} + \mathbf{I}\mathbf{g}_{Q-1} \end{pmatrix} \quad (15)$$

$$\begin{pmatrix} \mathbf{A} & & & & \\ & \mathbf{A} & & & \\ & & \ddots & & \\ & & & \mathbf{A} & \end{pmatrix} \begin{pmatrix} \phi_1 \\ \phi_3 \\ \vdots \\ \phi_{Q-1} \end{pmatrix} = \begin{pmatrix} \mathbf{g}_1 - \mathbf{I}\phi_2 \\ -\mathbf{I}\phi_2 + \mathbf{g}_3 - \mathbf{I}\phi_4 \\ \vdots \\ \mathbf{g}_Q - \mathbf{I}\phi_{Q-2} \end{pmatrix} \quad (16)$$

Since Equation (15) has the same form as Equation (14) the odd-even reduction can be performed recursively until one equation is left. The solution of the final equation can then be substituted in reverse order.

When ordering a 3D image slice by slice, the extension from 2D to 3D is straightforward. In Equation (14) \mathbf{A} now simply becomes $\mathbf{A} = \mathbf{K}_{2D} - 2\mathbf{I}$.

2.4 Other solvers

Other techniques to solve the linear system represented by Equation (6) include the Jacobi and Gauss-Seidel method. Cyclic reduction produces an exact result for the chosen discretization of the derivatives, whereas the Jacobi method gives approximated results.⁶ Because the rows of the matrix in Equations (12) and (14) all sum up to zero, these matrices are not strictly diagonally dominant and thus the Gauss-Seidel method cannot be used to solve this system.⁷ The fastest way to solve the system of Equation (6) is to use two steps of cyclic reduction to reduce the system to a quarter of the original size and then apply the Fourier analysis technique. By using only 2 steps of cyclic reduction the propagation of rounding errors in the right hand side vectors of Equation (15) and (16) is also kept at an acceptable level. This combination is naturally called FACR.⁴

3. EXPERIMENTS

To demonstrate the effect of the method and show its performance, three types of experiments were done. Firstly we used synthetic displacement fields together with synthetic and medical images with and without the addition of noise. Secondly we applied our method to a clinical application. Lastly we investigated the performance of our algorithm with respect to the required computation time.

3.1 Synthetic displacement fields

For the first experiments we created displacement fields, which we know to be solenoidal and applied them to both a synthetic and a medical image to obtain deformed images. The registration error was determined by averaging the length of the difference vector that was found by subtracting the displacement field found by the registration algorithm from the known true solenoidal deformation. We choose the following solenoidal deformation field:

$$\begin{pmatrix} A_x \sin(\omega_x y) \\ A_y \sin(\omega_y x) \\ A_z \sin(\omega_z x) \end{pmatrix} \quad (17)$$

where A_x , A_y and A_z are the amplitudes and ω_x , ω_y and ω_z are the frequencies in respectively the x, y and z direction. A visualisation of this field together with the deformed images is given in the left column of Figure 1.

The synthetic image contains a slowly varying checker board pattern and the medical image is part of the dynamic MR liver series. The deformed images were non-rigidly registered to their originals and the resulting displacement field were analysed with respect to their divergence.

A translation registration is used to initialise a multi resolution non rigid registration that uses Mutual Information as a similarity metric and B-splines to model the transformations. The used registration algorithm is based on the work of Mattes *et al.*⁸ Thévenaz *et al.*⁹ and Rueckert *et al.*¹⁰ The algorithm to remove the divergence was implemented using routines from the open source Insight Segmentation and Registration Toolkit¹¹ and Fortran routines from FishPack library in the Netlib mathematical software repository.

By adding noise to the test images, the correspondence between the images is reduced and the registration becomes more difficult. We investigated whether our method can correct for the expected increase in registration errors. Gaussian noise with varying variance was added to the synthetic image and the Signal to Noise Ratio was calculated according to:

$$SNR = 20^{10} \log \left(\frac{\gamma}{\sigma} \right) \quad (18)$$

where γ is the dynamic range of the synthetic image and σ is the standard deviation of the applied Gaussian noise.

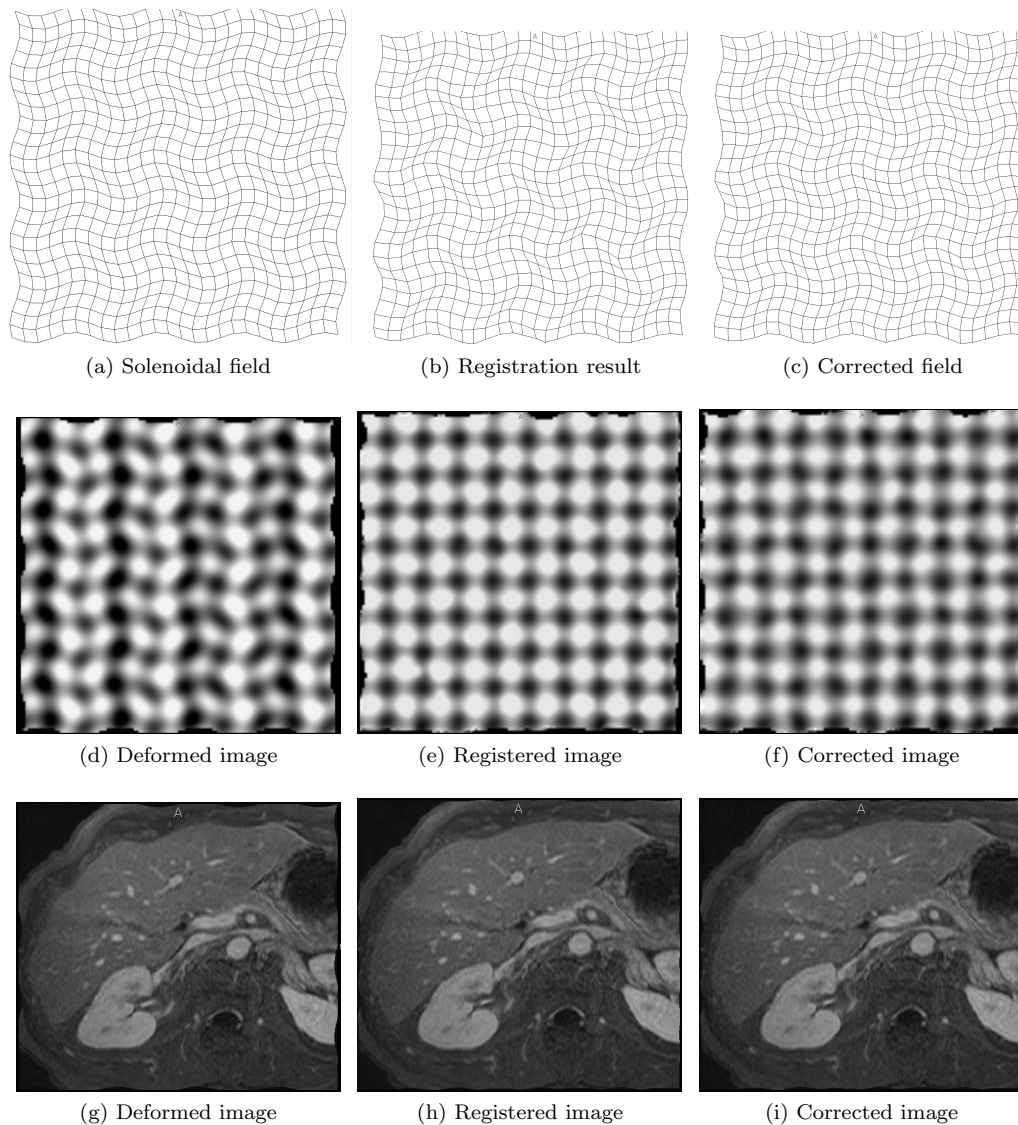


Figure 1: The left column shows the applied solenoidal displacement field and the corresponding deformed images, the middle column shows the registration results with on the top row the displacement field for the synthetic image and in the right column the divergence in the displacement field was removed.

3.2 Clinical application

In dynamic liver studies the registration of incompressible tissue plays an important role.¹² These registrations would normally have to be done in order to construct voxel-based time-intensity curves that are used for pharmacokinetic modelling of contrast agent uptake in a tumour, which can *e.g.* be used to assess its malignancy. The used data set consisted of five dynamic MR liver series. Each of these series contained six 3D MR images acquired at a fixed interval of about 30 seconds. For each series all images were put into registration with the 3rd time point and the resulting displacement field was corrected for volume changes. In total 25 registrations and corrections were performed. We analysed the divergence that was present in both the uncorrected and the corrected displacement fields

3.3 Performance tests

In the last type of experiments we measured the calculation time required for removing the divergence of displacement fields of various sizes. These experiments were performed on a 64 bit machine with a 2.3 GHz AMD processor and 16 GB of RAM.

4. RESULTS

The second column of Figure 1 shows the displacement field and the accordingly deformed images, found by registration of the synthetically deformed images shown in the first column. In the last column the corrected field and images are displayed. As can be seen from this figure, the corrected field shows more regularity and resembles the original field better. This becomes more apparent when we calculate the divergence of both fields in each point. Figure 2 shows a slice of this divergence image from both the unconstrained and the corrected field.

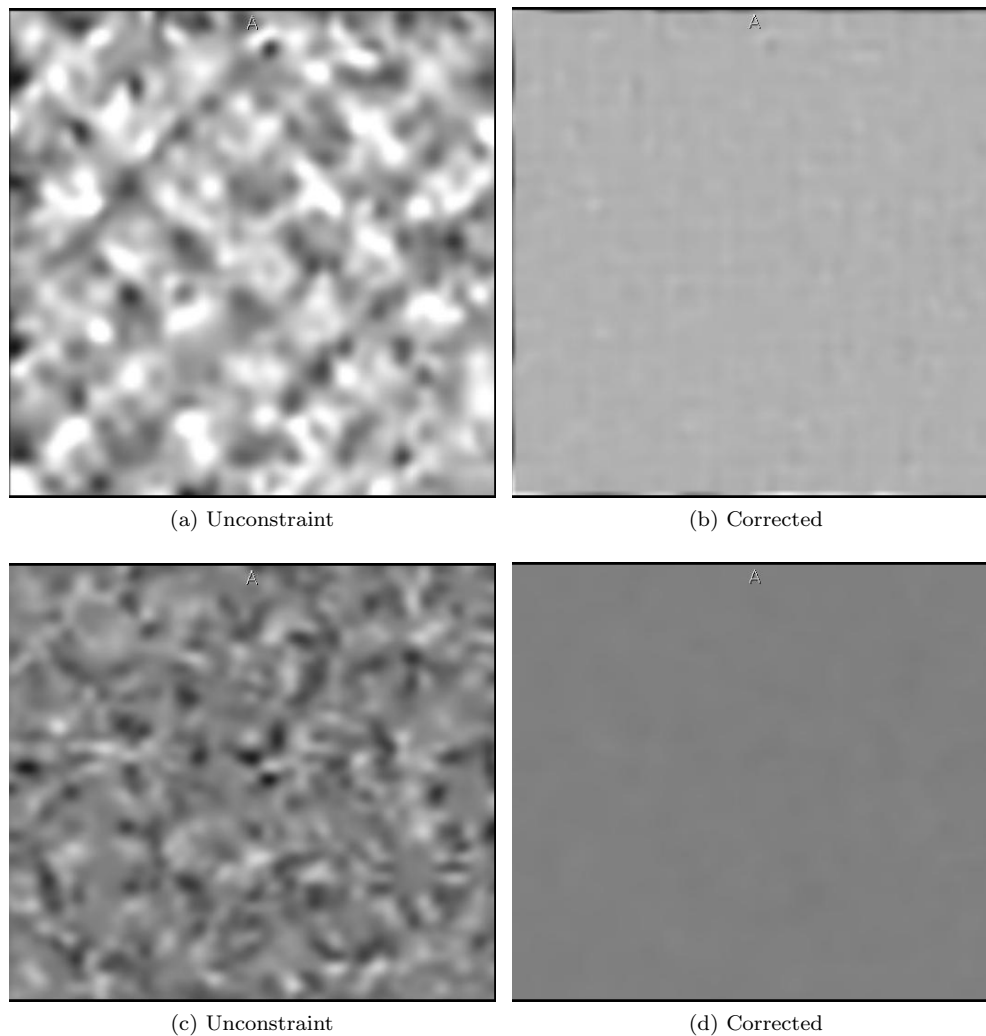


Figure 2: A slice showing the divergence of the uncorrected (left) and corrected (right) field of both the synthetic (top row) and the medical image (bottom row). The contrast and brightness values of both images are the same.

The average absolute divergence present in both the uncorrected and corrected field is listed in Table 1. After correction the divergence in the field is reduced by about one order of magnitude.

| Image | Divergence | |
|-----------|---------------------------------|---------------------------------|
| | uncorrected | corrected |
| Synthetic | 0.151 ± 0.003 | $(1.27 \pm 0.05) \cdot 10^{-2}$ |
| Medical | $(7.96 \pm 0.05) \cdot 10^{-2}$ | $(3.55 \pm 0.02) \cdot 10^{-3}$ |

Table 1: Reduction in divergence for for both the synthetic and the medical image

Adding noise to the image slightly increases the divergence that is present in the displacement field after registration, as can be seen in Figure 3. After post-processing this increase in local volume change is removed.

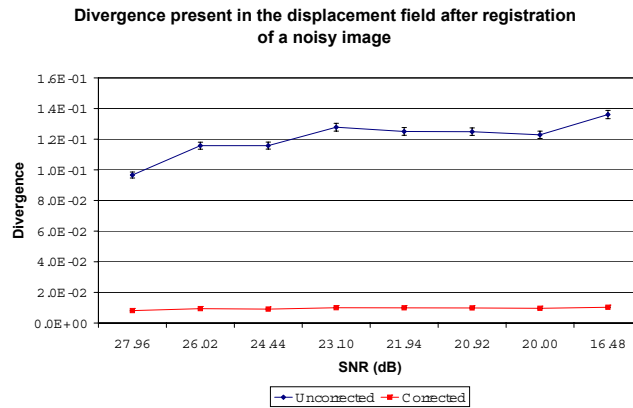


Figure 3: Divergence in the registered displacement field slightly increases with the noise level in the image, but our method can reduce it to the same level again.

By looking at the average registration error in Figure 4 we see that the registration improves a bit by removing the divergence from the displacement field found by the unconstrained registration algorithm.

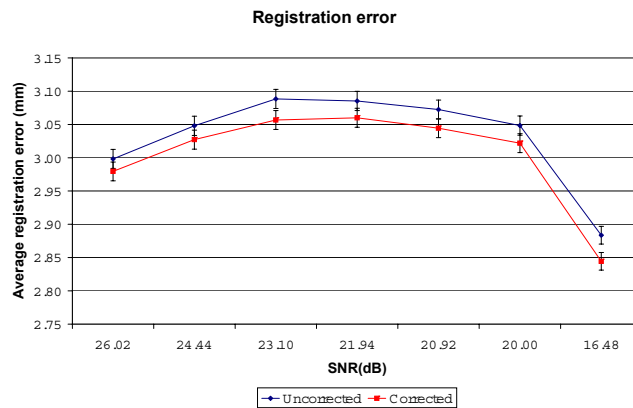


Figure 4: Error in the registration before and after correction for unwanted volume changes

Table 2 lists the results from the registration of the dynamic MR liver series. The displayed values are the average absolute value of the divergence that occurs in the displacement field for the uncorrected and the corrected case. The average reduction of the divergence, due to our method is up to 3 orders of magnitude

The results of the performance experiments are presented in Figure 5, where the computation times are plotted against the size of one dimension of the images. All images had equal size in each of the three dimensions. From

| | T | Divergence | |
|-----------|---|----------------------------------|---------------------------------|
| | | Uncorrected | Corrected |
| Patient 1 | 0 | $(2.78 \pm 0.02) \cdot 10^{-2}$ | $(9.05 \pm 0.08) \cdot 10^{-5}$ |
| | 1 | $(1.58 \pm 0.01) \cdot 10^{-2}$ | $(7.08 \pm 0.07) \cdot 10^{-5}$ |
| | 2 | $(1.35 \pm 0.01) \cdot 10^{-2}$ | $(6.23 \pm 0.07) \cdot 10^{-5}$ |
| | 4 | $(7.76 \pm 0.07) \cdot 10^{-3}$ | $(3.90 \pm 0.04) \cdot 10^{-5}$ |
| | 5 | $(9.62 \pm 0.08) \cdot 10^{-3}$ | $(4.67 \pm 0.04) \cdot 10^{-5}$ |
| Patient 2 | 0 | $(2.15 \pm 0.02) \cdot 10^{-2}$ | $(1.47 \pm 0.01) \cdot 10^{-5}$ |
| | 1 | $(4.36 \pm 0.04) \cdot 10^{-2}$ | $(3.11 \pm 0.03) \cdot 10^{-5}$ |
| | 2 | $(1.91 \pm 0.01) \cdot 10^{-2}$ | $(1.28 \pm 0.01) \cdot 10^{-5}$ |
| | 4 | $(3.28 \pm 0.02) \cdot 10^{-2}$ | $(1.91 \pm 0.02) \cdot 10^{-5}$ |
| | 5 | $(12.12 \pm 0.08) \cdot 10^{-3}$ | $(7.68 \pm 0.06) \cdot 10^{-6}$ |
| Patient 3 | 0 | $(7.27 \pm 0.07) \cdot 10^{-2}$ | $(4.80 \pm 0.05) \cdot 10^{-5}$ |
| | 1 | $(6.06 \pm 0.06) \cdot 10^{-2}$ | $(4.08 \pm 0.04) \cdot 10^{-5}$ |
| | 2 | $(2.24 \pm 0.01) \cdot 10^{-2}$ | $(1.47 \pm 0.01) \cdot 10^{-5}$ |
| | 4 | $(3.76 \pm 0.04) \cdot 10^{-2}$ | $(2.77 \pm 0.02) \cdot 10^{-5}$ |
| | 5 | $(2.21 \pm 0.02) \cdot 10^{-2}$ | $(1.76 \pm 0.02) \cdot 10^{-5}$ |
| Patient 4 | 0 | $(3.38 \pm 0.03) \cdot 10^{-2}$ | $(3.01 \pm 0.02) \cdot 10^{-5}$ |
| | 1 | $(7.23 \pm 0.06) \cdot 10^{-2}$ | $(6.74 \pm 0.06) \cdot 10^{-5}$ |
| | 2 | $(1.92 \pm 0.01) \cdot 10^{-2}$ | $(1.57 \pm 0.01) \cdot 10^{-5}$ |
| | 4 | $(1.34 \pm 0.01) \cdot 10^{-2}$ | $(1.24 \pm 0.01) \cdot 10^{-5}$ |
| | 5 | $(5.92 \pm 0.05) \cdot 10^{-3}$ | $(6.07 \pm 0.05) \cdot 10^{-6}$ |
| Patient 5 | 0 | $(6.59 \pm 0.06) \cdot 10^{-2}$ | $(5.49 \pm 0.06) \cdot 10^{-5}$ |
| | 1 | $(4.02 \pm 0.03) \cdot 10^{-2}$ | $(3.79 \pm 0.03) \cdot 10^{-5}$ |
| | 2 | $(3.53 \pm 0.02) \cdot 10^{-2}$ | $(2.52 \pm 0.02) \cdot 10^{-5}$ |
| | 4 | $(2.08 \pm 0.02) \cdot 10^{-2}$ | $(1.50 \pm 0.01) \cdot 10^{-5}$ |
| | 5 | $(2.85 \pm 0.02) \cdot 10^{-2}$ | $(2.36 \pm 0.02) \cdot 10^{-5}$ |

Table 2: Mean absolute values of the divergence in the uncorrected and corrected displacement field in a registered dynamic MR liver series

the three steps - calculation of the divergence, solving Poissons equation and calculation of the gradient - the first and last step always take approximately the same time while solving Poissons equation always takes the longest time. For images smaller than $200 \times 200 \times 200$, the total computation time is less than 40 seconds, with larger images the computation time increases rapidly. However the computation time per voxel stays approximately the same: $3\mu s$. When we compare the computation time of our post-processing step to those of the registration, which typically take hours, it is neglectable. The used algorithms were not optimised for speed and did not use any parallel processing of the data. By using multiple processors its is very well possible to gain speed in all of the above mentioned calculation steps.

5. CONCLUSION

In this paper we describe a method to remove volume changes from a displacement field. Although the techniques have been applied in the field of fluid dynamics, the application to image registration is new. The described method can be used as post-processing stage for any registration algorithm. Our experiments show that by applying this technique on the displacement field found by a non rigid registration algorithm, we are able to reduce the divergence in the field by a factor 10-1000. In initial experiments, we also found that this post-processing step slightly improved the accuracy of image registration. Compared to the registration, the computational costs of this post-processing step are neglectable.

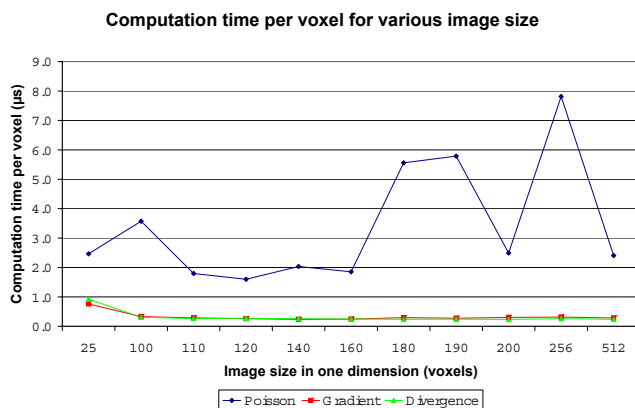


Figure 5: Computation times of the various steps in the proposed method to remove the divergence in a vector field.

REFERENCES

1. T. Rohlfing, C. Maurer Jr., D. Bluemke, and M. Jacobs, "Volume-preserving nonrigid registration of mr breast images using free-form deformation with an incompressibility constraint," *IEEE Transactions On Medical Imaging* **22**, pp. 730–741, June 2003.
2. T. Rohlfing, C. M. Jr., D. Bluemke, and M. Jacobs, "An alternating-constraints algorithm for volume-preserving nonrigid registration of contrast-enhanced MR mammography images," in *WBIR 2003, LNCS* **2717**, pp. 291–300, 2003.
3. E. Haber and J. Modersitzki, "Numerical methods for volume preserving image registration," *Inverse Problems* **20**(5), pp. 1621–1638, 2004.
4. P. N. Swarztrauber, *Fast Poisson Solver*, vol. 24, The mathematical Association of America, Washington, DC, 1984.
5. G. Strang, *Applied Mathematics and Scientific Computing*, Wellesley-Cambridge Press, 2007.
6. N. Black and S. Moore, "Jacobi method," *From MathWorld-A Wolfram Web Resource* **1**, p. 1, 2006.
7. N. Black and S. Moore, "Gauss-Seidel method," *From MathWorld-A Wolfram Web Resource* **1**, p. 1, 2006.
8. D. Mattes, D. Haynor, H. Vesselle, T. Lewellen, and W. Eubank, "PET-CT image registration in the chest using free-form deformations," *IEEE Transactions On Medical Imaging* **22**, pp. 120–128, Jan. 2003.
9. P. Thevenaz and M. Unser, "Optimization of mutual information for multiresolution image registration," *IEEE Transactions On Image Processing* **9**, pp. 2083–2099, Dec. 2000.
10. D. Rueckert, L. Sonoda, C. Hayes, D. Hill, M. Leach, and D. Hawkes, "Nonrigid registration using free-form deformations: Application to breast mr images," *IEEE Transactions On Medical Imaging* **18**, pp. 712–721, August 1999.
11. L. Ibanez, W. Schroeder, L. Ng, and J. Cates, *The ITK Software Guide*. Kitware, Inc. ISBN 1-930934-15-7, <http://www.itk.org/ItkSoftwareGuide.pdf>, second ed., 2005.
12. K. A. Saddi, C. Chef'd'hotel, and F. Cheriet, "Large deformation registration of contrast-enhanced images with volume-preserving constraint," in *Medical Imaging 2007: Image Processing*, J. P. W. Pluim and J. M. Reinhardt, eds., **6512**, March 2007.